Infilling of Missing Rainfall Radar Data with a Memory-Assisted Deep Learning Approach

Johannes Meuer[1], Laurens M. Bouwer[2], Frank Kaspar[3], Roman Lehmann[4], Wolfgang Karl[4], Thomas Ludwig[1], and Christopher Kadow[1]

[1]German Climate Computing Center (DKRZ), Hamburg, Germany
[2]Climate Service Center Germany (GERICS), Helmholtz-Zentrum Hereon, Hamburg, Germany
[3]Deutscher Wetterdienst (DWD), Offenbach, Germany
[4]Karlsruhe Institute of Technology (KIT), Karlsruhe, Germany

Correspondence: Johannes Meuer (meuer@dkrz.de)

Abstract. Incomplete spatio-temporal meteorological observations can result in misinterpretations of the current climate state, uncertainties in early warning systems, or inaccuracies in nowcasting models and can thereby pose signficant challanges in hydrology research or similar applications. Traditional statistical methods for infilling missing precipitation data demand substantial computational resources and fail over large areas with sparse data - like temporary outages of weather radars. Although recent machine learning advancements have shown promise in addressing missing meteorological or satellite observations, they typically focus on spatial aspects, overlooking the complex spatio-temporal variability characteristic of precipitation, especially during extreme events. We propose a deep convolutional neural network enhanced with a temporal memory component to better account for temporal changes in precipitation fields. This approach can analyse arbitrary sequences from before and/or after the incomplete observation of interest. Our model is trained and evaluated on the hourly RADKLIM dataset, which features 1-km resolution precipitation derived from combined radar and weather station data across Germany. By infilling both synthetic and actual data gaps of RADKLIM, the study demonstrates the model's effectiveness, providing detailed insights into its capabilities during significant rainfall events, such as those in May 2012 and July 2021, including those responsible for the Ahrtal flood. This novel approach represents a step forward in hydrological applications, potentially improving the way we predict and manage water-related events by increasing the accuracy and reliability of precipitation data analysis.

1 Introduction

The process of producing accurate climate information is crucial for informing policy as well as for applications in various sectors, e.g. water management or agriculture. For example, nowcasting of events such as thunderstorms, heavy rainfall and snowfall plays a vital role in assessing and planning the management of water resources, flood hazards, urban runoff and climate variability for long-term trends (James et al., 2018; Lang, 2002; Wapler et al., 2012; Teegavarapu et al., 2018). Precipitation data collected by weather radars are an important source of information for such applications, but the reliability and accuracy of these applications depend heavily on the quality of the data. However, temporally and spatially continuous systems are often plagued by outages that lead to missing values (Teegavarapu et al., 2018; Geiss and Hardin, 2021; Kadow et al., 2020;

Barrios et al., 2018) and radars in particular are prone to technical challenges such as blocking of radar beams and near-ground dead zones (Winterrath et al., 2017; Geiss and Hardin, 2021). To illustrate this, consider figure 6, which shows three data samples taken from the RADKLIM dataset of Germany's meteorological service DWD (Winterrath et al., 2018). This dataset is generated using a process that merges radar observations with weather station measurements to produce continuous spatial and temporal precipitation pattern data across Germany at different temporal resolutions (5min and 1hr). However, due to outages, the radars were not able to monitor precipiation in the shaded grey areas, as shown in the figure.
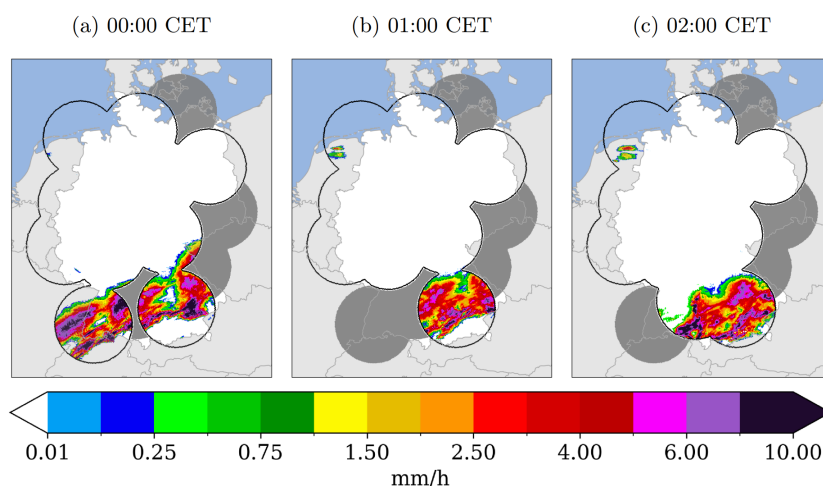
Figure 1. Examples of missing precipitation recordings after radar outages in the RADKLIM dataset on June 24th 2002 of three sequential hours. The grey regions highlight the radars that failed to record any precipitation.

Such problems can lead to misinterpretation or increased uncertainty in observations and predictions. Methods to fill gaps in climate data range from statistical approaches such as spatial interpolation (Smith et al., 1996; Oliver and Webster, 1990; Teegavarapu et al., 2018; Simanton and Osborn, 1980; Teegavarapu and Chandramouli, 2005; Verworn and Haberlandt, 2011) and linear regression (Vislocky and Fritsch, 1995) to machine learning approaches such as support vector machines (Landot et al., 2008). *Kriging* (Oliver and Webster, 1990), *Inverse Distance Weighting* (Simanton and Osborn, 1980) and *Linear Weight Optimisation Method* (Teegavarapu et al., 2018) provide good estimates for point-wise reconstructions, but their ability to provide good spatial reconstructions is limited by nearby existing values. This is also shown by Verworn and Haberlandt (2011), who estimate spatial precipitation patterns in northern Germany based on nearby weather stations and radar images. Using only weather stations and statistical reconstruction methods results in overly smooth precipitation maps, while including additional radar information results in much more realistic spatial patterns. Their study highlights not only the limitations of statistical approaches to spatial reconstruction, but also the importance of spatially complete radar images.

Data-driven image inpainting is used to repair image damage caused by raindrops, to improve the quality of old images, or to increase the resolution of low-quality images (Yu et al., 2018; Liu et al., 2018; Elharrouss et al., 2020), but also to fill gaps in climate data. For example, Shibata et al. (2018) use inpainting to reconstruct incomplete satellite images of sea surface

temperatures, and Geiss and Hardin (2021) propose a generative adversarial network (GAN) to fill gaps in patchy radar images. Kadow et al. (2020) apply partial convolutions (Liu et al., 2018) to reconstruct missing values in global surface temperature

45 grids. Partial convolutions are able to reconstruct missing values in arbitrarily shaped regions, which is particularly useful when dealing with missing observational data.

While data-driven techniques have shown promising results, they only take into account the spatial relationships in the data, not the temporal variability. On the other hand, while statistical approaches take into account data distributions from the past, they lack the ability to reconstruct spatial features, especially when considering large regions with missing values. To address

50 these limitations, we propose a data-driven image inpainting model that is capable of reconstructing arbitrarily shaped missing value regions, while also taking into account the temporal relationships in the data.

The remainder of this paper is organized as follows: Section 2 describes the datasets used and the methodological framework implemented for the infilling of missing precipitation data. Section 3 presents the experimental results and provides a comprehensive discussion of the performance of the proposed models. Finally, Section 4 summarizes the key findings of the

55 study and discusses potential future research directions. The appendices provide additional details on the models' architectures, evaluation metrics, experimental overview, and additional results.

2 Data and methods

2.1 Data

This study is based on the RADKLIM-dataset of Deutscher Wetterdienst (DWD; Germany's national meteorological service).

60 RADKLIM is a data set of reprocessed gauge-adjusted radar data (Winterrath et al., 2017, 2018). DWD operates a network of 17 weather radars (C-band; Lengfeld et al. (2019)) as well as a network of several hundred ground-based rain gauges (Kaspar and Mächel, 2023). Weather radars send pulses of electromagnetic energy into the atmosphere and measure reflectivity to monitor the movement, intensity and type of precipitation, such as rain, snow and hail. However, radars cannot observe precipitation directly. In contrast, rain gauges can only provide incomplete spatial information of precipitation events, pending on the density

65 of the network. To derive quantitative precipitation estimates (QPEs), the signals from weather radars can be combined with measurements from the rain gauges. To provide timely information, esp. for water management applications, DWD derives QPEs in real-time by adjusting radar observations with data from the German rain gauge network (RADOLAN: Radar Online Adjustment). The information is stored as precipitation intensities with an intensity resolution of 0.1 mm and a spatial resolution of 1 km^2 resulting in a 900x1100 km grid for Germany, and is provided in real time within 30 minutes of the last measurement.

70 The data are provided at five-minute and hourly time frequencies. The products might contain gaps caused by outages of radars, e.g. due to technical failures or regular maintenance. The archived collection of operationally produced RADOLAN data is also inhomogeneous in time as it was produced with the current hardware and software configuration at the time of creation. To provide a dataset suitable for climatological application, the radar reflectivities have been reprocessed (i.e., the same set of algorithms for artefacts and attenuation correction as well as adjustments to rain gauge observations has been applied) to

75 create a homogeneous set of precipitation observations covering the period from 2001 onwards ("RADKLIM", Lengfeld et al. (2019)). In this study we focus on the hourly grids of RADKLIM (Winterrath et al., 2018) for training and evaluation.

2.2 Model

2.2.1 Image Inpainting U-Net

We use an image inpainting U-net (Ronneberger et al., 2015) as a baseline model for reconstructing missing value regions in
80 precipitation data. This model takes a single precipitation grid as input. Each data sample contains an observed precipitation grid with no missing values (i.e. the original RADKLIM data, considered as 'ground truth' in our analysis), a binary missing value mask, and a masked grid obtained by element-wise multiplication of the original observations and the mask. This allows us to simulate missing value regions in complete radar images. We replace conventional convolutional operations in the U-net with partial convolutions by Liu et al. (2018). The automatic mask updating mechanism in these operations efficiently
85 handles irregularly shaped holes in missing value masks, outperforming other methods trained only on regularly shaped holes. Equation 1 defines partial convolution operations that show improved inpainting results, especially for large and irregularly shaped missing value regions. The first term describes the masking of the input data I with the mask M and applies a scaling factor depending on the number of ones in M. The weight matrix W represents the trainable weights of the network. The second term describes the mechanism for updating the mask after each convolution. If the convolution has been able to apply
90 its output to at least one valid input value, that position is marked as valid. The architecture of our baseline CNN is illustrated in Appendix A1.

$$
\begin{aligned}
i' &= \begin{cases} W^T(I \circ M)\frac{sum(1)}{sum(M)} + b, & if\, sum(M) > 0 \\ 0, & otherwise \end{cases} \\
m' &= \begin{cases} 1, & if\, sum(M) > 0 \\ 0, & otherwise \end{cases}
\end{aligned}
\tag{1}
$$

2.2.2 Temporal Memory Module

95 Precipitation estimation is a challenging spatio-temporal problem, as it involves highly non-linear patterns in both time and space. To incorporate temporal information, we propose a straightforward channel-based approach that includes sequences of precipitation grids within the input data, rather than considering only grids of single timesteps. We can arbitrarily define the number of time steps to consider. The dimension of the channel is equal to the number of time steps considered as input data. The output of the network is a tensor representing a reconstructed precipitation grid for a single time step. The detailed
100 architecture can be seen in Appendix A2.

This channel-based approach has limitations in distinguishing between long-term and short-term relationships in the data. To address this, Xingjian et al. (2015) proposed a convolutional long short-term memory (LSTM) network for precipitation nowcasting, which extends the original fully connected LSTM architecture of Hochreiter and Schmidhuber (1997) with convo-

lutional structures. The network takes as input a sequence of time-continuous precipitation grids collected from weather radars.
105 The equations of the fully connected LSTM are modified to incorporate convolutional operations, given by Equations 2.

$$f_t = \sigma(W_{fx} * X_t + W_{fh} * H_{t-1} + W_{fc} \circ C_{t-1} + b_f)$$
$$i_t = \sigma(W_{ix} * X_t + W_{ih} * H_{t-1} + W_{ic} \circ C_{t-1} + b_i)$$
$$g_t = tanh(W_{gx} * Xt + W_{gh} * H_{t-1} + b_g)$$
$$C_t = f_t \circ C_{t-1} + i_t \circ g_t$$
110 $$o_t = \sigma(W_{ox} * X_t + W_{oh}H_{t-1} + W_{oc} \circ + b_o)$$
$$h_t = o_t \circ tanh(C_t) \tag{2}$$

The Ws and bs are weights and biases that are learned by the model. The memory states C_t, C_{t-1}, the hidden states H_t, H_{t-1} and the gates f_t, i_t, o_t, g_t are represented as three-dimensional matrices, with input channels in the first dimension and a two-dimensional spatial precipitation field in the other two dimensions. The Hadamard product is denoted by $\circ$ and the
115 convolutional operation is denoted by $*$. The convolutional LSTM is implemented in an encoder-decoder architecture similar to the future predictor model proposed by Srivastava et al. Srivastava et al. (2015). The combination of spatial data processing using CNNs and sequential data processing using LSTMs has been shown to outperform each technique used individually.

Instead of processing the data sequences in the channel dimension, the input sequence is iteratively passed through the set of equations 2. Note that these operations are applied only to the precipitation tensors, not to the mask tensors. Similar to the
120 autoencoder of Srivastava et al. (2015), the decoder reconstructs the input sequence in reverse order. As a result, the output tensors from the encoder are provided to the decoder in reverse order. This speeds up the weight optimisation, as the model primarily considers short-range correlations Srivastava et al. (2015). Appendix A3 shows how we implemented the LSTM module.

3   Results and discussion

125 Due to radar outages, which are still quite common, many grids from the RADKLIM dataset contain missing values. We have therefore created a dataset containing only complete radar images where no radar outages have occurred, and a dataset containing missing values where radar outages have occurred. In addition, the DWD introduced three new radar stations in 2014/2015 to the original 14 radar stations to improve spatial coverage. Therefore, we performed separate analyses on data from only 14 radars over the complete time range and from all 17 radars from 2015 onwards. An overview of the different
130 experiments can be found in Appendix C1, where we trained three models on each experiment: the baseline, channel-based and LSTM architectures.

In order to comprehensively evaluate our three proposed models, we have selected a single missing value mask covering a significant area in central Germany for the first experiment. This gap was caused by three radar outages in January 2012, resulting in a three-hour data absence (see Appendix G). The chosen area presents an additional challenge as it encompasses

135 the Harz Mountains, renowned for intricate precipitation patterns influenced by terrain (Panziera et al., 2011). Our performance
evaluation relies on a range of metrics: (1) root mean square error (RMSE in mm/h), (2) absolute mean error (AME in mm/h),
(3) temporal correlation over spatial mean ($r_{xy,time}$), (4) mean spatial correlation ($\overline{r_{xy,space}}$), and (5) spatial correlation of
sum over time ($r_{xy,sum}$). Detailed explanations of these calculations are provided in Appendix B. The models were trained on
complete grids from 2001 to 2022 covered by 14 radars and excluding the evaluation years, utilizing the missing data mask

140 from Appendix G. We specifically chose the years 2007, 2012, and 2016, which were not part of the training data, to allow
meaningful comparisons across three distinct annual cycles. Metrics were then computed by infilling simulated missing values
for 2007, 2012, and 2016 with the same mask and averaging the results across these years.

Figure 2 (detailed in Table D1 shows that the channel-based model outperforms the baseline model in terms of pixel-wise
(RMSE) and average (AME) precipitation reconstruction and maintains a good temporal correlation. However, the baseline

145 model outperforms the channel-based model in terms of spatial metrics ($\overline{r_{xy,space}}$ and $r_{xy,sum}$), indicating that it is better at
reconstructing the spatial distribution per time step as well as the total amount of precipitation at a fixed location. This may
be due to the under-estimation of precipitation in the channel-based approach, which can be seen in figure 3. The final model
including the temporal memory module is the best performing model with the highest scores for temporal, spatial and summed
correlations, and lowest errors (RMSE and AME).

150 We further explore the results of the first experiment using scatter plots in Figure 4, which provides a visual comparison
between the model predictions and the observations. The baseline approach exhibits the largest spread with respect to the
spatial average precipitation, while the channel approach underestimates especially average fields with low precipitation. Here,
the LSTM model provides the most accurate results. In the matter of reconstructing the temporal average at each grid point,
the results of the baseline model feature the worst overall approximation and major outliers between 0.05 and 0.1 mm/h,

155 indicating over-estimation of precipitation at specific grid points. The channel-based approach reduces the number of outliers
in this range but still exhibits overestimations between 0.1 and 0.15 mm/h, as well as underestimations at most grid points.
The LSTM provides the best estimations for the in time averaged grid points being closest to the red line with much smaller
outliers.

In Figure 5, we make a visual comparison of reconstructed grids for this single missing value mask scenario. Here, we

160 consider a rainfall event from May 2012. The results from the channel-based approach again show an underestimation of
precipitation during the event. On the other hand, the baseline and LSTM approaches give very similar results compared to
the original RADKLIM data. However, the LSTM has some artificial checkerboard patterns, which were also observed by Liu
et al. (2018) from the original partial convolutions.

In the second experiment, we trained the three models on all the complete hourly data from 2001-2022 covered by 14 radars.

165 We extracted a mask dataset by setting all missing values from the remaining incomplete hourly data to zero and the existing
values to one. During training, we combined the complete data with all the extracted missing value masks. This gave us the
most reliable models for infilling real case scenarios with missing values. Figure 6 shows a visual comparison of infilled images
generated by the baseline and LSTM models from the June 2002 radar outages, where we have no original observations. The
baseline model was provided with a single time step for each infill application, while the LSTM was additionally provided with
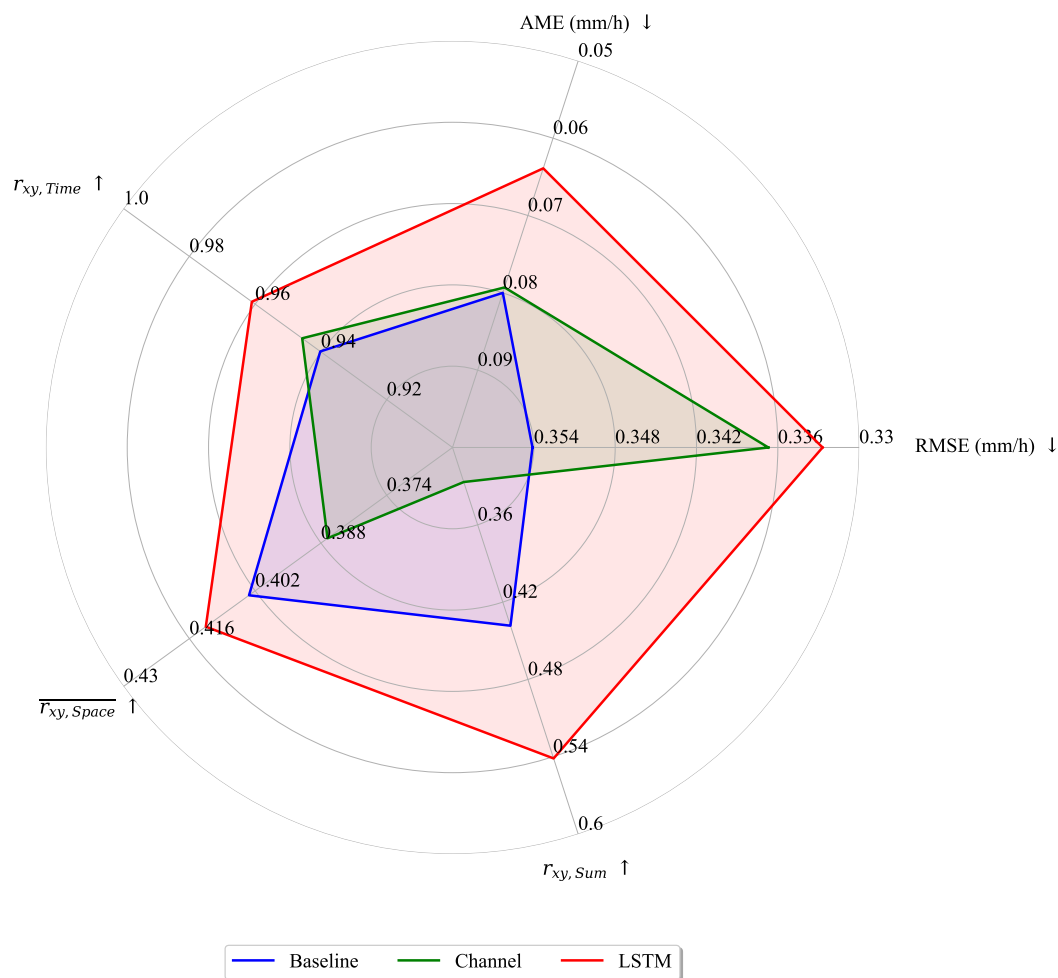
Figure 2. Verification metrics of the baseline model (blue) with the channel-based memory approach (green) and the advanced temporal memory module (red). The ↑ determines that a high - and the ↓ a low value should be aimed for.

the two previous and subsequent time steps. Comparing images (a) and (b) from the baseline model (centre), a large region of precipitation disappears within one hour. In contrast, the LSTM model is able to preserve this by incorporating the temporal information of the previous two hours. It is clear that the LSTM model produces the most realistic results, while the spatial patterns are also best approximated with this model.

In our final experiment, we looked at a recent flood event caused by extreme precipitation, training our models on complete data from 2015-2018, covered by all 17 radars. In July 2021, Germany was hit by massive rainfall events and the resulting floods caused more than 180 deaths and billions of euros in damage. The return period of the 24h rainfall is estimated to be around a 500 years, with an even longer return period in the most affected area (Mohr et al., 2023).
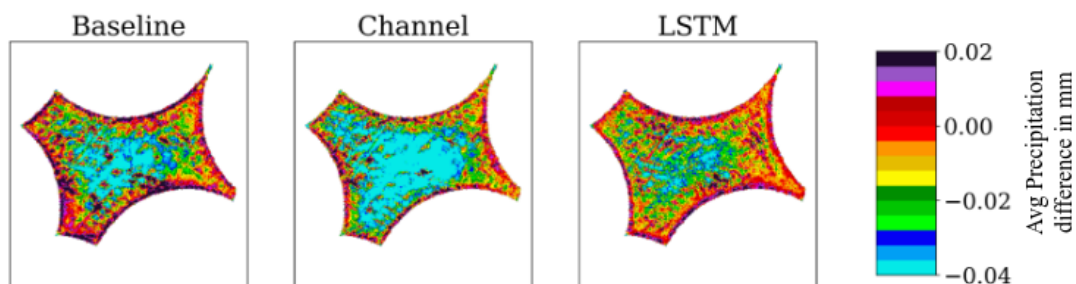
Figure 3. Average difference between the predicted precipitation in the infilled area and the actual precipitation measured. The field is an average of all infilled grids from 2007, 2012 and 2016. A negative value means that too little precipitation was predicted and a positive value means that too much was predicted.
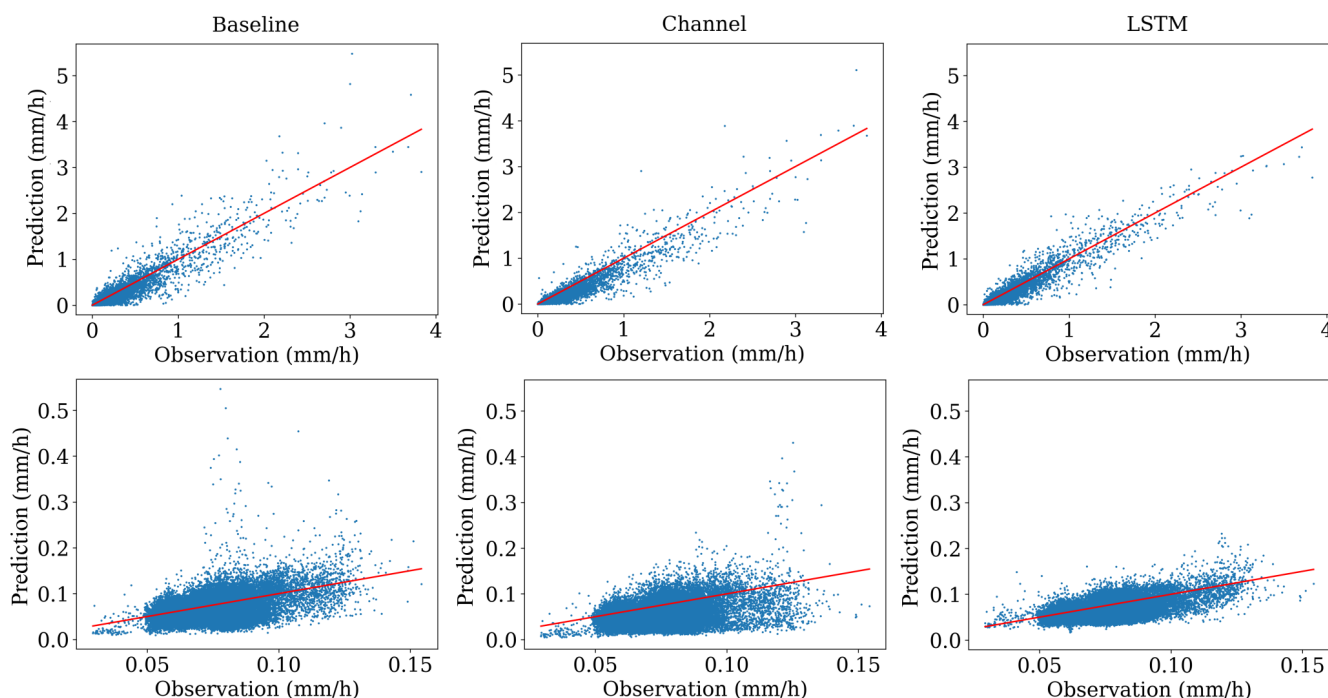
Figure 4. The top row shows the spatial average of precipitation for each time step from 2007, 2012 and 2016. The bottom row shows the temporal average of all grids in 2007, 2012 and 2016 for each grid point. Both calculations were performed on the infilled area only. The red line marks the optimal results.

Figure E1 shows a snapshot of this rainfall event (top row), where we have masked out a large region of precipitation west of the location of the largest flooding (Ahr river basin) and applied the LSTM model to infill this region. We have also applied the infilling of this region to 20 consecutive hours of the extreme rainfall event and show the accumulated rainfall over this period

180
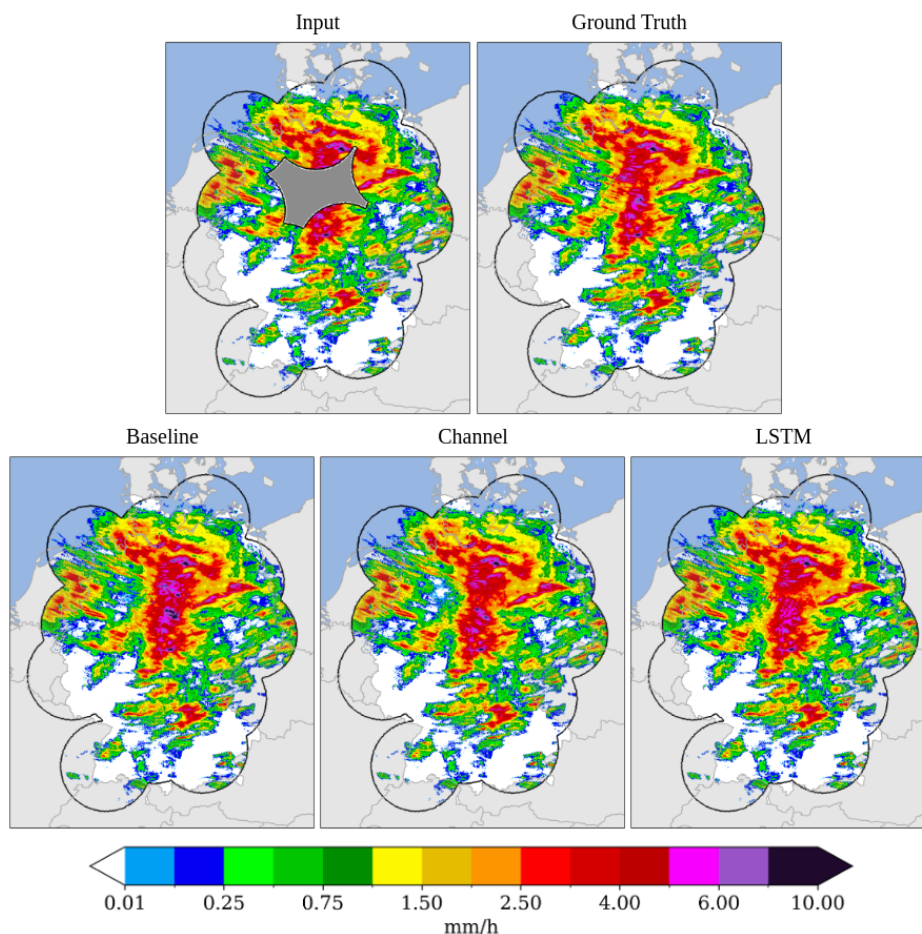
Figure 5. The top row shows the input to the models (simulated missing value region in grey) and the original RADKLIM data. The bottom row shows the infilled grids from our three models. This exact event was recorded on 31st May 2012 18:00 CET.

(bottom row). A complete map of the event and the reconstruction can be seen in Appendix E. Here we can see a limitation of our model, which leads to an underestimation of the extreme rainfall. The model predicts a total rainfall of 70.76 mm in the Ahr basin over the 20 hour period, whereas the original observed rainfall was 101.89 mm. This amounts to an accuracy of 69.5 %. However, in the event of radar failure during such events, our method could still potentially provide an estimate of rainfall over the affected region based on nearby radar data and help improve flood forecasting and risk assessment.

The evaluation of the proposed models shows that the LSTM model outperforms the baseline and channel-based approaches in terms of overall accuracy. The model consistently improves performance across all evaluation metrics (figure 2), as well as through visual analysis of scatter plots in figure 4 and infilled images in figure 6. However, it should be noted that the LSTM model also requires significantly more hardware resources and computing time for training compared to the other models.
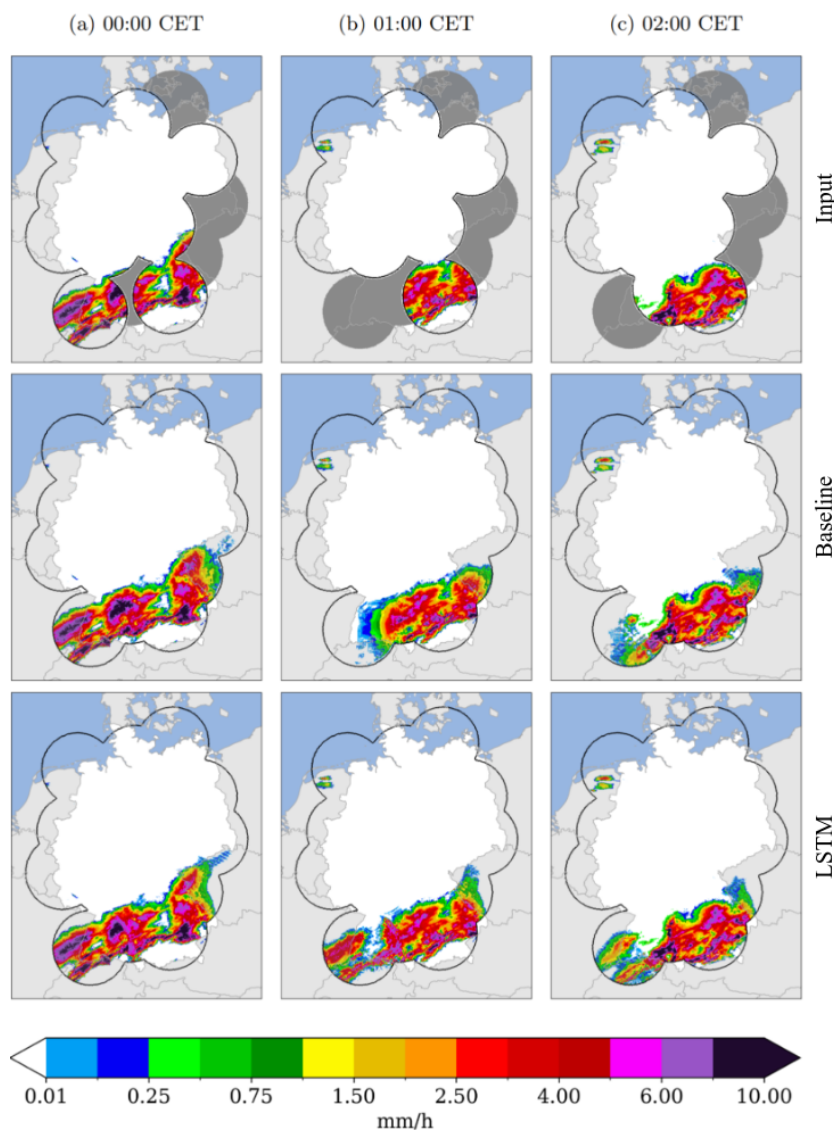
Figure 6. Comparison of the patchy rainfall records (top row) used as input to our infilling models with the reconstructed results from the baseline model (centre row) and the LSTM model (bottom row).

190   This may impact the feasibility and scalability of implementing the LSTM model in certain operational settings with limited computing resources. Hence, a careful trade-off analysis may be necessary when choosing the most appropriate model for a specific application.

    In the final step, we filled in all hourly data from 2001 to 2022 using our LSTM model, which was trained on data from 17 radar stations. This enhanced dataset extends radar coverage to periods before 2014, ensuring both spatial and temporal
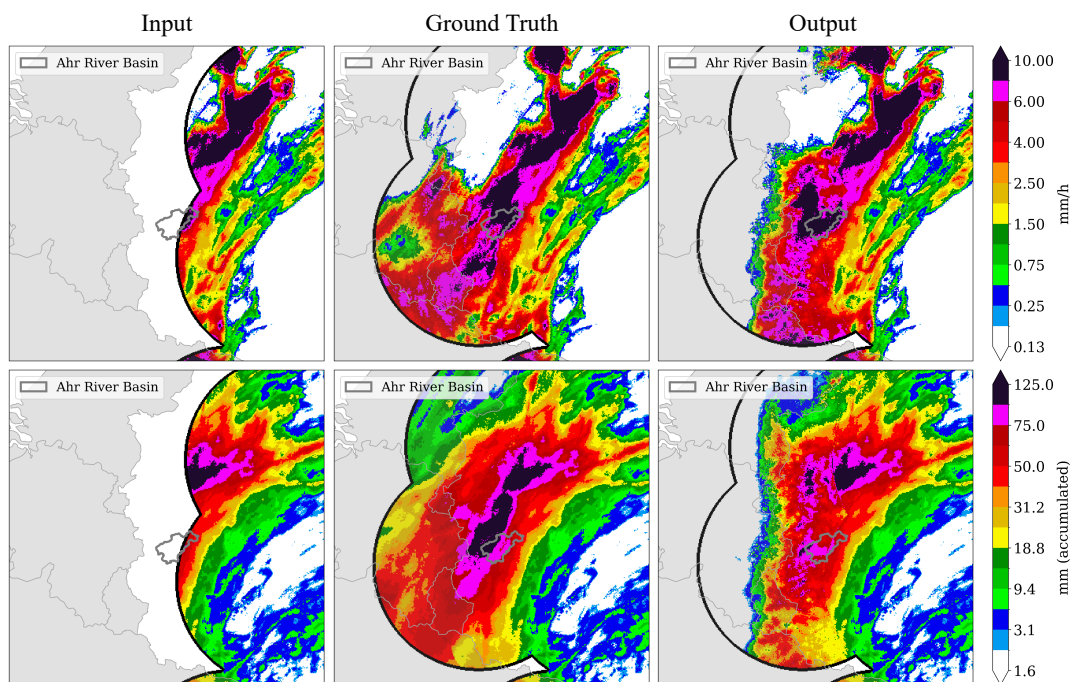
Figure 7. Illustration of the extreme precipitation event in the Ahrtal on the 14th July in 2021. The Ahr river basin is highlighted by gray border. Here we compare the original RADKLIM data with the output of the LSTM model. The top maps show a reconstruction of a single hour (18:00 CET) in mm/h, the bottom row shows the accumulated amount of precipitation in mm from reconstructions over 20 hours (between 2:00 and 21:00 hrs. on 14 July, 2021).

consistency. The infilled dataset will be made available for public access upon publication of this study. A few selected samples from this dataset are shown in Appendix G1.

4 Conclusions

We proposed and evaluated three machine learning models for infilling missing precipitation data: A basic inpainting model, a straightforward channel-based approach that considers a sequence of time steps as input, and an LSTM approach as an advancement to the channel-based approach. The results of the evaluation showed that the LSTM model outperforms the baseline and channel-based approaches in terms of overall performance, the baseline model has a larger prediction error, and the channel-based model has a tendency to underestimate precipitation. However, the LSTM model also requires significantly more hardware resources and computing time compared to the other models, while the other models already perform quite well. Increasing the complexity of the model can improve the results, with the understanding that it requires more resources than other models. Our analysis highlights the potential of machine learning models to be used for efficiently infilling missing

precipitation data. The tangible advantage of employing the infilled data generated by our models requires exploration through an examination of how it might enhance the accuracy and performance of other nowcasting models that depend on the same dataset. Future applications of our research could include a cascaded approach, using the baseline model for immediate results, the channel-based model for better temporal estimation, and finally the best results with the LSTM model with the largest

210   latency. We also see scope for additional applications, beyond the infilling of missing radar data. By combining information on observed rainfall data from rain gauges, additional spatial information could be gained and the accuracy of the rainfall information can be improved.

Code and data availability.   The code used for the analysis and simulations in this study is openly accessible at: https://github.com/FREVA-CLINT/ climatereconstructionAI. The repository contains scripts written in Python, along with detailed documentation to facilitate replication and

215   further exploration of the methodologies employed. The data utilized in this research were obtained from the Germany's meteorological service (Deutscher Wetterdienst, DWD). Hourly radar-based precipitation data (RADOLAN/RADKLIM) covering the study period are available under an open data license: http://dx.doi.org/10.5676/DWD/RADKLIM_RW_V2017.002. A fully infilled version next to the original data of the hourly precipitation data will be made available to the public upon publication of this study.

Appendix A: Model
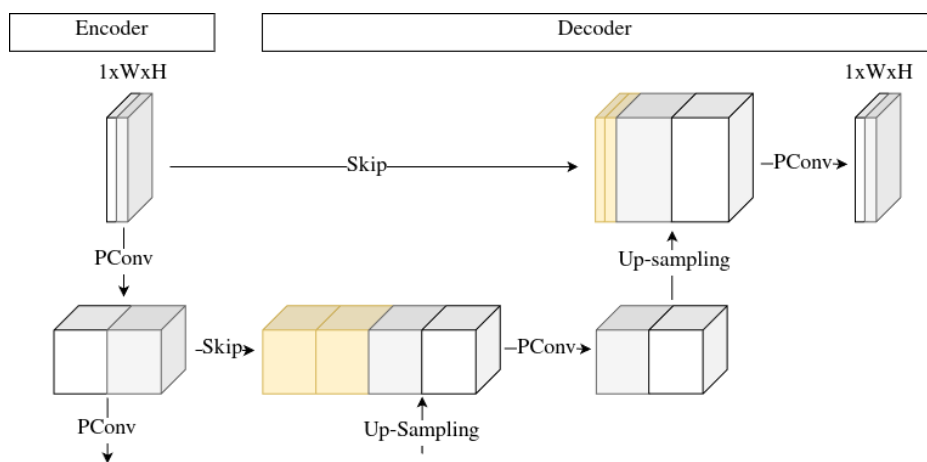
Figure A1. The architecture of the baseline model.
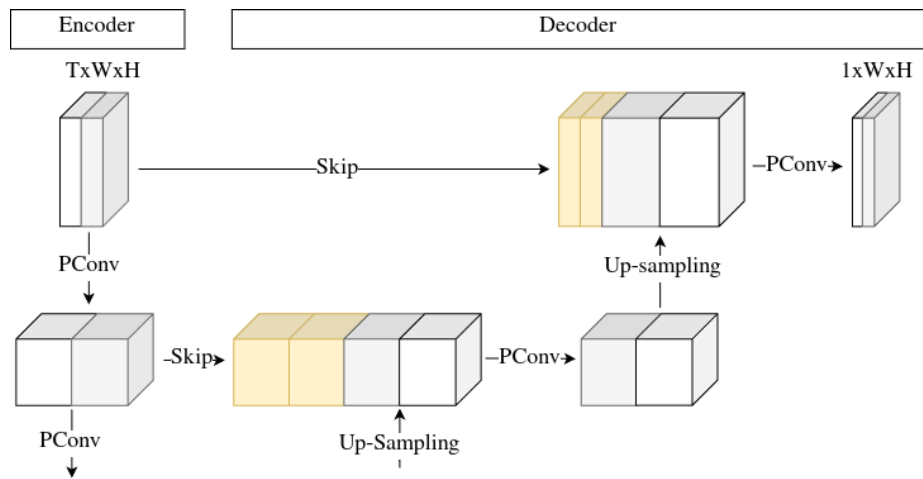
Figure A2. The architecture of the channel-based model.
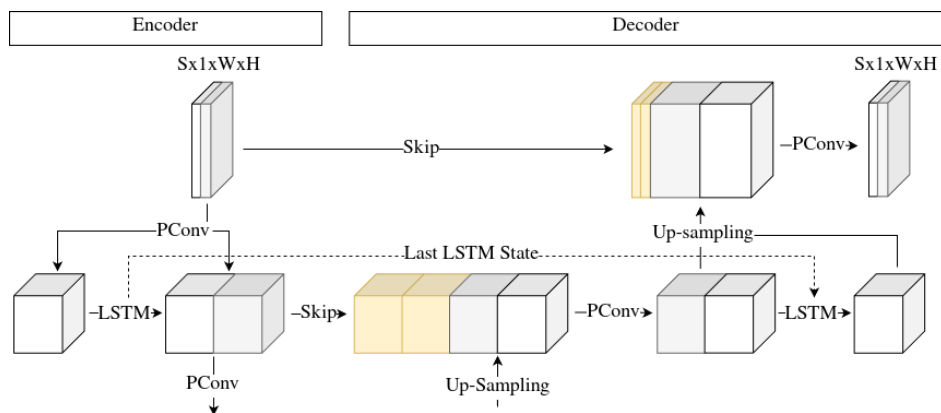
Figure A3. The architecture of the LSTM model.

Appendix B: Formulas

$$RMSE = \sqrt{\frac{1}{N \cdot W \cdot H} \sum_{t=0}^{N-1} \sum_{i=0}^{W-1} \sum_{j=0}^{H-1} (x_{t,i,j} - y_{t,i,j})^2} \tag{B1}$$

$$AME = |\frac{1}{N} \cdot \sum_{t=0}^{N-1} (\frac{1}{W \cdot H} \sum_{i=0}^{W-1} \sum_{j=0}^{H-1} x_{t,i,j} - \frac{1}{W \cdot H} \sum_{i=0}^{W-1} \sum_{j=0}^{H-1} y_{t,i,j})| \tag{B2}$$

$$r_{xy,Time} = \frac{\sum_{t=0}^{N-1} T_{x,t} \cdot T_{y,t} - \overline{T_x} \cdot \overline{T_y}}{\sqrt{(\sum_{t=0}^{N-1} T_{x,t}^2 - \overline{T_x})(\sum_{t=0}^{N-1} T_{y,t}^2 - \overline{T_y})}} \tag{B3}$$

$$r_{xy,Space} = \frac{\sum_{i=0}^{W \cdot H-1} x_{t,i} \cdot y_{t,i} - \overline{x_t} \cdot \overline{y_t}}{\sqrt{(\sum_{i=0}^{W \cdot H-1} x_{t,i}^2 - \overline{x_t})(\sum_{i=0}^{W \cdot H-1} y_{t,i}^2 - \overline{y_t})}} \tag{B4}$$

$$r_{xy,Sum} = \frac{\sum_{i=0}^{W \cdot H-1} \Sigma(x_i) \cdot \Sigma(y_i) - \overline{\Sigma(y_i)} \cdot \overline{\Sigma(y)}}{\sqrt{(\sum_{i=0}^{W \cdot H-1} \Sigma(x_i)^2 - \overline{\Sigma(x)})(\sum_{i=0}^{W \cdot H-1} \Sigma(y_i)^2 - \overline{\Sigma(y)})}} \tag{B5}$$

Appendix C: Experiment Overview

Table C1. An overview of all experiments that we performed.

Experiment	Training time range	Evaluation time range	Training samples	Evaluation samples	Radar Coverage
1 - Single Mask	2001-2022[1]	2007, 2012, 2016	55989	26328	14
2 - All Masks	2001-2022	2001-2022	82317	87263	14
3 - Ahrtal	2015-2018	2021	15647	20	17

1 Excluding years 2007, 2012 and 2016

Appendix D: Metric Results

Table D1. Verification metrics of the baseline model, the channel-based memory approach, and the advanced LSTM approach. The ↑ in the columns determines that a high - and the ↓ a low value should be aimed for. The bold text highlights the best performing model in the channel based models and the advanced approaches.

Model	RMSE ↓	AME ↓	$r_{xy,Time}$ ↑	$\overline{r_{xy,Space}}$ ↑	$r_{xy,Sum}$ ↑
Baseline	0.3541	0.08	0.9402	0.4033	0.4383
Channel	0.3367	0.0793	0.9457	0.3866	0.3268
LSTM	**0.3327**	**0.0639**	**0.961**	**0.4125**	**0.5413**

Appendix E: Ahrtal Results
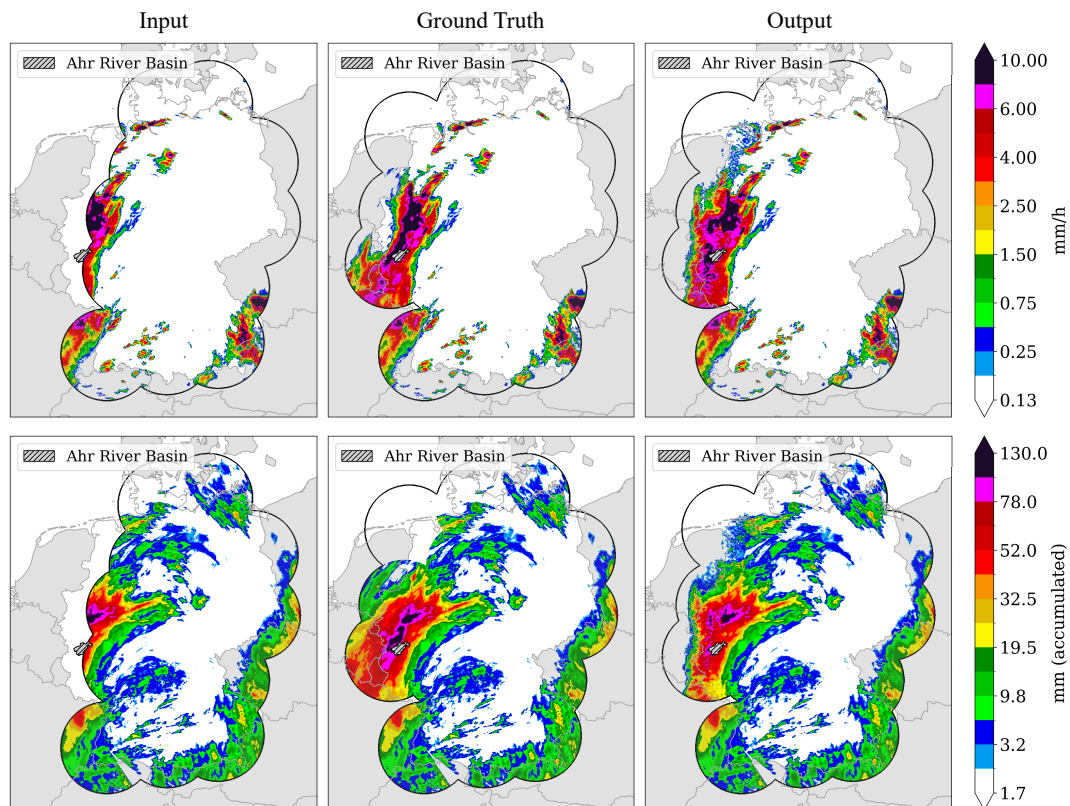
Figure E1. Illustration of the extreme precipitation event in the Ahrtal on the 14th July in 2021. The Ahr river basin is highlighted by gray hatching. Here we compare the original RADKLIM data with the output of the LSTM model. The top maps show a reconstruction of a single hour (18:00 CET) in mm/h, the bottom row shows the accumulated amount of precipitation in mm from reconstructions over 20 hours (between 2:00 and 21:00 hrs. on 14 July, 2021).

Appendix F: Training Mask
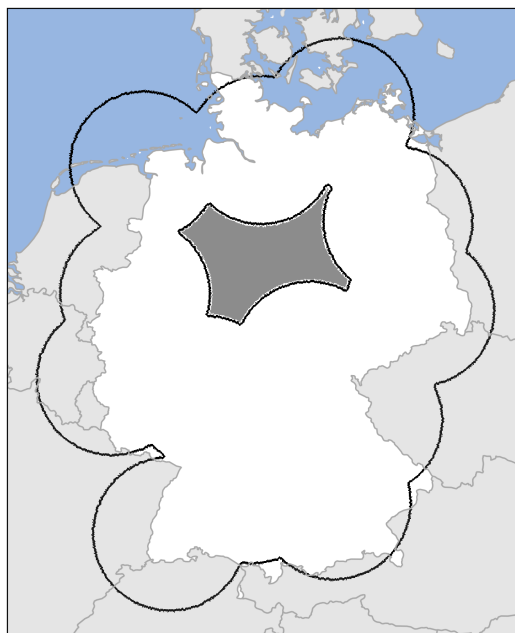
Figure F1. Real case study of radar outages that occurred in January 2012. Four overlapping radars failed at the same time, causing a large region with missing values (grey) in the precipitation recording.

Appendix G: Infilled Samples
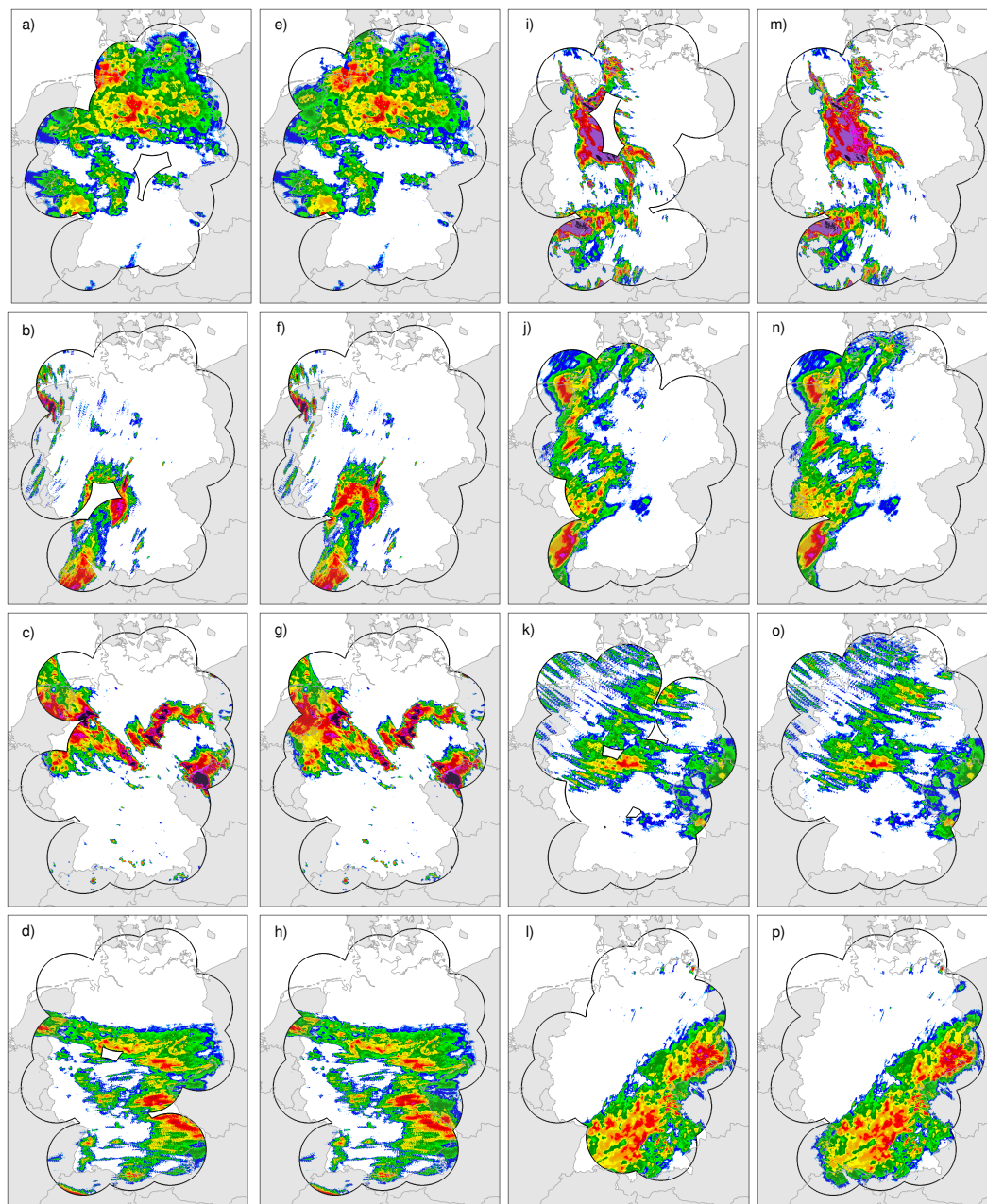
Figure G1. A selection of infilled samples using the LSTM model. a)-d) and i)-l) show samples from the original dataset, and e)-h) and m)-p) the corresponding infilled versions.

Author contributions. Johannes Meuer conceived the study, designed the research methodology, conducted data analysis, and collected and processed the data used in the study. All authors contributed to the interpretation of results and provided critical feedback throughout the manuscript preparation. All authors contributed to the writing and editing of the manuscript.

Competing interests. The authors of this article declare that no competing interests are present.

235   *Acknowledgements.* The authors are grateful to the German Climate Computing Center (DKRZ) for providing the hardware for the calculations and to the Germany's meteorological service (DWD) for providing the RADKLIM data that were used for this study. Johannes Meuer, Roman Lehmann and Wolfgang Karl acknowledge support by the Karlsruhe Institute of Technology (KIT). Thomas Ludwig and Christopher Kadow are funded from the German Climate Computing Center (DKRZ). Laurens Bouwer acknowledges support by the Helmholtz Association under the research program "Changing Earth – Sustaining our Future".

References

Barrios, A., Trincado, G., and Garreaud, R.: Alternative approaches for estimating missing climate data: application to monthly precipitation records in South-Central Chile, Forest Ecosystems, 5, 1–10, 2018.

Elharrouss, O., Almaadeed, N., Al-Maadeed, S., and Akbari, Y.: Image inpainting: A review, Neural Processing Letters, 51, 2007–2028, 2020.

Geiss, A. and Hardin, J. C.: Inpainting Radar Missing Data Regions with Deep Learning, Atmospheric Measurement Techniques Discussions, pp. 1–28, 2021.

Hochreiter, S. and Schmidhuber, J.: Long short-term memory, Neural computation, 9, 1735–1780, 1997.

James, P. M., Reichert, B. K., and Heizenreder, D.: NowCastMIX: Automatic integrated warnings for severe convection on nowcasting time scales at the German Weather Service, Weather and Forecasting, 33, 1413–1433, 2018.

Kadow, C., Hall, D. M., and Ulbrich, U.: Artificial intelligence reconstructs missing climate information, Nature Geoscience, 13, 408–413, 2020.

Kaspar, F. and Mächel, H.: Beobachtung von Klima und Klimawandel in Mitteleuropa und Deutschland, Brasseur, G.P., Jacob, D., Schuck-Zöller, S. (eds) Klimawandel in Deutschland, https://doi.org/10.1007/978-3-662-66696-8_3, 2023.

Landot, T., Sgellari, S., Lima, C., and Lall, U.: In-filling missing historical daily rainfall data study, Final Report, South Florida Water Management District, Columbia University, New York, NY, 2008.

Lang, P.: Konrad, Umweltwissenschaften und Schadstoff-Forschung, 14, 212, 2002.

Lengfeld, K., Winterrath, T., Junghänel, T., Hafer, M., and Becker, A.: Characteristic spatial extent of hourly and daily precipitation events in Germany derived from 16 years of radar data; Characteristic spatial extent of hourly and daily precipitation events in Germany derived from 16 years of radar data, Meteorologische Zeitschrift, 28, 363–378, 2019.

Liu, G., Reda, F. A., Shih, K. J., Wang, T.-C., Tao, A., and Catanzaro, B.: Image inpainting for irregular holes using partial convolutions, in: Proceedings of the European Conference on Computer Vision (ECCV), pp. 85–100, 2018.

Mohr, S., Ehret, U., Kunz, M., Ludwig, P., Caldas-Alvarez, A., Daniell, J. E., Ehmele, F., Feldmann, H., Franca, M. J., Gattke, C., et al.: A multi-disciplinary analysis of the exceptional flood event of July 2021 in central Europe. Part 1: Event description and analysis, Nat. Hazards Earth Syst. Sci., 23, 525–551, https://doi.org/10.5194/nhess-23-525-2023, 2023.

Oliver, M. A. and Webster, R.: Kriging: a method of interpolation for geographical information systems, International Journal of Geographical Information System, 4, 313–332, 1990.

Panziera, L., Germann, U., Gabella, M., and Mandapaka, P.: NORA–Nowcasting of Orographic Rainfall by means of Analogues, Quarterly Journal of the Royal Meteorological Society, 137, 2106–2123, 2011.

Ronneberger, O., Fischer, P., and Brox, T.: U-net: Convolutional networks for biomedical image segmentation, in: International Conference on Medical image computing and computer-assisted intervention, pp. 234–241, Springer, 2015.

Shibata, S., Iiyama, M., Hashimoto, A., and Minoh, M.: Restoration of sea surface temperature satellite images using a partially occluded training set, in: 2018 24th International Conference on Pattern Recognition (ICPR), pp. 2771–2776, IEEE, 2018.

Simanton, J. R. and Osborn, H. B.: Reciprocal-distance estimate of point rainfall, Journal of the Hydraulics Division, 106, 1242–1246, 1980.

Smith, T. M., Reynolds, R. W., Livezey, R. E., and Stokes, D. C.: Reconstruction of historical sea surface temperatures using empirical orthogonal functions, Journal of Climate, 9, 1403–1420, 1996.

Srivastava, N., Mansimov, E., and Salakhudinov, R.: Unsupervised learning of video representations using lstms, in: International conference on machine learning, pp. 843–852, PMLR, 2015.

Teegavarapu, R. S. and Chandramouli, V.: Improved weighting methods, deterministic and stochastic data-driven models for estimation of missing precipitation records, Journal of hydrology, 312, 191–206, 2005.

280 Teegavarapu, R. S., Aly, A., Pathak, C. S., Ahlquist, J., Fuelberg, H., and Hood, J.: Infilling missing precipitation records using variants of spatial interpolation and data-driven methods: use of optimal weighting parameters and nearest neighbour-based corrections, International Journal of Climatology, 38, 776–793, 2018.

Verworn, A. and Haberlandt, U.: Spatial interpolation of hourly rainfall–effect of additional information, variogram inference and storm properties, Hydrology and Earth System Sciences, 15, 569–584, 2011.

285 Vislocky, R. L. and Fritsch, J. M.: Generalized additive models versus linear regression in generating probabilistic MOS forecasts of aviation weather parameters, Weather and Forecasting, 10, 669–680, 1995.

Wapler, K., Goeber, M., and Trepte, S.: Comparative verification of different nowcasting systems to support optimisation of thunderstorm warnings, Advances in Science and Research, 8, 121–127, 2012.

Winterrath, T., Brendel, C., Hafer, M., Junghänel, T., Klameth, A., Walawender, E., Weigl, E., and Becker, A.: Erstellung einer radargestützten
290 Niederschlagsklimatologie, 2017.

Winterrath, T., Brendel, C., Hafer, M., Junghänel, T., Klameth, A., Lengfeld, K., Walawender, E., Weigl, E., and Becker, A.: RADKLIM Version 2017.002: Reprocessed gauge-adjusted radar data, one-hour precipitation sums (RW), Deutscher Wetterdienst (DWD), 2018.

Xingjian, S., Chen, Z., Wang, H., Yeung, D.-Y., Wong, W.-K., and Woo, W.-c.: Convolutional LSTM network: A machine learning approach for precipitation nowcasting, in: Advances in neural information processing systems, pp. 802–810, 2015.

295 Yu, J., Lin, Z., Yang, J., Shen, X., Lu, X., and Huang, T. S.: Generative image inpainting with contextual attention, in: Proceedings of the IEEE conference on computer vision and pattern recognition, pp. 5505–5514, 2018.